Darling–Dennison resonance and Coriolis coupling in the bending overtones of the A A u 1 state of acetylene, C 2 H 2

Anthony J. Merer, Nami Yamakita, Soji Tsuchiya, Adam H. Steeves, Hans A. Bechtel, and Robert W. Field

Citation: The Journal of Chemical Physics **129**, 054304 (2008); doi: 10.1063/1.2939246
View online: http://dx.doi.org/10.1063/1.2939246
View Table of Contents: http://scitation.aip.org/content/aip/journal/jcp/129/5?ver=pdfcov
Published by the AIP Publishing

Darling–Dennison resonance and Coriolis coupling in the bending overtones of the $\tilde{A}\,^1A_u$ state of acetylene, C_2H_2

Anthony J. Merer,[1,2] Nami Yamakita,[3] Soji Tsuchiya,[4] Adam H. Steeves,[5] Hans A. Bechtel,[6] and Robert W. Field[5,a)]

[1]*Institute of Atomic and Molecular Sciences, Academia Sinica, Taipei 10617, Taiwan*
[2]*Department of Chemistry, University of British Columbia, Vancouver, British Columbia V6T 1Z1, Canada*
[3]*Department of Chemical and Biological Sciences, Japan Women's University, Mejirodai, Bunkyo-ku, Tokyo 112-8681, Japan*
[4]*Department of Applied Chemistry and Institute of Molecular Science, National Chiao Tung University, Hsinchu 30010, Taiwan*
[5]*Department of Chemistry, Massachusetts Institute of Technology, Cambridge, Massachusetts 02139, USA*
[6]*Advanced Light Source Division, Lawrence Berkeley National Laboratory, Berkeley, California 94720, USA*

(Received 27 March 2008; accepted 13 May 2008; published online 4 August 2008)

Rotational analyses have been carried out for the overtones of the ν_4 (torsion) and ν_6 (in-plane cis-bend) vibrations of the $\tilde{A}\,^1A_u$ state of C_2H_2. The $v_4+v_6=2$ vibrational polyad was observed in high-sensitivity one-photon laser-induced fluorescence spectra and the $v_4+v_6=3$ polyad was observed in IR-UV double resonance spectra via the ground state ν_3 (Σ^+_u) and $\nu_3+\nu_4$ (Π_u) vibrational levels. The structures of these polyads are dominated by the effects of vibrational angular momentum: Vibrational levels of different symmetry interact via strong *a*-and *b*-axis Coriolis coupling, while levels of the same symmetry interact via Darling–Dennison resonance, where the interaction parameter has the exceptionally large value $K_{4466}=-51.68$ cm^{-1}. The *K*-structures of the polyads bear almost no resemblance to the normal asymmetric top patterns, and many local avoided crossings occur between close-lying levels with nominal *K*-values differing by one or more units. Least squares analysis shows that the coupling parameters change only slightly with vibrational excitation, which has allowed successful predictions of the structures of the higher polyads: A number of weak bands from the $v_4+v_6=4$ and 5 polyads have been identified unambiguously. The state discovered by Scherer *et al.* [J. Chem. Phys. **85**, 6315 (1986)], which appears to interact with the $K=1$ levels of the 3^3 vibrational state at low *J*, is identified as the second highest of the five $K=1$ members of the $v_4+v_6=4$ polyad. After allowing for the Darling–Dennison resonance, the zero-order bending structure can be represented by $\omega_4=764.71$, $\omega_6=772.50$, $x_{44}=0.19$, $x_{66}=-4.23$, and $x_{46}=11.39$ cm^{-1}. The parameters x_{46} and K_{4466} are both sums of contributions from the vibrational angular momentum and from the anharmonic force field. For x_{46} these contributions are 14.12 and -2.73 cm^{-1}, respectively, while the corresponding values for K_{4466} are -28.24 and -23.44 cm^{-1}. It is remarkable how severely the coupling of ν_4 and ν_6 distorts the overtone polyads, and also how in this case the effects of vibrational angular momentum outweigh those of anharmonicity in causing the distortion. © *2008 American Institute of Physics*.
[DOI: 10.1063/1.2939246]

I. INTRODUCTION

The $\tilde{A}\,^1A_u-\tilde{X}\,^1\Sigma^+_g$ electronic transition of acetylene is one of the most widely studied of all polyatomic spectra. The principal reason is that acetylene is the simplest compound containing a C≡C triple bond, so that analysis of the spectrum gives a clear picture of what happens on $\pi^*\leftarrow\pi$ electronic excitation of such a bond. As is well known, acetylene is linear in its ground electronic state, but, as was shown by Ingold and King[1,2] and by Innes[3] over 50 years ago, it becomes trans-bent in its first singlet excited state $\tilde{A}\,^1A_u$. This was one of the first demonstrations that a molecule can change its point group on electronic excitation. In fact, it is more complicated than this. The first singlet excited state (S_1), which corresponds to a $^1\Sigma^-_u$ state of the linear molecule, has potential minima corresponding to both *cis*- and *trans*-bent isomers,[4–11] but transitions from the ground state are only permitted to levels of the *trans*-isomer by the dipole selection rules. The S_1 state of the *cis*-isomer, $\tilde{A}\,^1A_2$, has never been observed, though it is calculated to lie about 3000 cm^{-1} higher than the $\tilde{A}\,^1A_u$ state of the *trans*-isomer[7,11] or roughly 1000 cm^{-1} below the dissociation limit.[12] Interesting dynamics will occur at the barrier to *cis-trans*-isomerization, and a search for the spectroscopic signatures of these dynamics has been one of the motivations for this work.

a)Author to whom correspondence should be addressed. Tel.: (617)253-1489. FAX: (617)253-7030. Electronic mail: rwfield@mit.edu.

A second reason for interest in the $\tilde{A}\,^1A_u - \tilde{X}\,^1\Sigma^+_g$ transition of acetylene is the wealth of detail it contains. The Franck–Condon pattern in absorption[13,14] consists of a long progression in the *trans*-bending (or "straightening") vibration ν_3, each member of which is the origin of a short progression in the C—C stretching vibration ν_2. This is consistent with the rotational analysis, which shows[15] that the equilibrium HCC angle is 122.5°, and that the C—C bond length has increased from 1.208 to 1.375 Å, which is greater than that in C_2H_4. One of the results of the change of point group on electronic excitation, which was found in the spectrum of acetylene for the first time, is "axis-switching,"[16] where a small rotation of the principal inertial axis system upon excitation causes the appearance of unexpected $K'-\ell''=0$ and ± 2 subbands in an otherwise perpendicular $(K'-\ell''=\pm 1)$ transition. Although predissociation sets in[12] just below the 3^4_0 band, its effects are minimal at first. Very extensive rotational analyses have therefore been possible, leading to a detailed description of the level structures of the ν_2 and ν_3 progressions and, from hot bands, of the ground state ν_4 (*trans*-bending) vibration.[13,14,17]

With a detailed understanding of the upper state level structure available, the $\tilde{A}\,^1A_u$ state has been a valuable stepping stone for emission studies,[18–23] and particularly for double resonance experiments. Among these are many comprehensive studies of the high vibrational levels of the ground state using stimulated emission pumping[24–27] and of the level structures of various Rydberg and valence states[28–30] and the acetylene cation.[31,32]

Interestingly, although the Franck–Condon active (gerade) vibrational levels are fairly well understood, much less is known about the ungerade vibrations of the $\tilde{A}\,^1A_u$ state. IR-UV double resonance experiments via the ground state $3\nu_3$ level[33,34] have allowed analyses of the three ungerade fundamentals, ν_4 (a_u, torsion), ν_5 (b_u, antisymmetric CH stretch), and ν_6 (b_u, in-plane *cis*-bend), together with the combination 3^15^1. The ν_4 and ν_6 fundamentals of the $\tilde{A}\,^1A_u$ state are almost degenerate,[33] with wavenumbers of 764.9 and 768.3 cm^{-1}, respectively; they are also extremely strongly coupled by Coriolis interactions. Further double resonance experiments via the ground state ν_3 fundamental have allowed analyses[35] of the combinations 3^24^1, 3^26^1, 3^34^1, and 3^36^1, where again the structure is massively distorted by Coriolis effects. The only other information about the ungerade vibrations comes from one-photon laser-induced fluorescence (LIF) studies of the excitation spectrum[36] where, with the help of supersonic jet-cooling, some weak bands in among the strong Franck–Condon progressions were identified as combinations involving overtones of the ν_4 and ν_6 vibrations.

The assignment of these weak combination bands[36] suggested that many other bands involving the low-lying ungerade vibrations ν_4 and ν_6 should be observable given sufficiently sensitive experiments. These bands would be highly forbidden according to the Franck–Condon principle, but could obtain small amounts of intensity through anharmonic interactions of their upper levels with the Franck–Condon allowed levels. The purpose of the present paper is to describe the successful observation of a number of such bands belonging to overtones of the ν_4 and ν_6 vibrations with up to five vibrational quanta. The gerade members have been observed in one-photon LIF experiments, and the ungerade members in IR-UV double resonance experiments via the ground state ν_3 and $\nu_3+\nu_4$ levels.

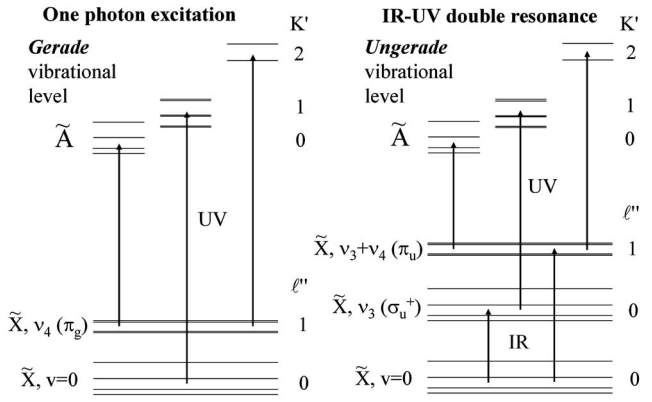

FIG. 1. Schematic energy level diagram showing how the $K'-\ell''=\pm 1$ selection rule necessitates two experiments, both in one-photon excitation and in IR-UV double resonance, in order to observe the complete set of upper state levels with $K'=0-2$.

The rotational and vibrational structures of these bands are highly unusual. Because the ν_4 and ν_6 vibrations have very nearly the same frequency, many of the features of a doubly degenerate vibration, with its associated vibrational angular momentum, appear in their overtone spectra. The strong Coriolis coupling of the ν_4 and ν_6 vibrations is one of these. Another is the strikingly large Darling–Dennison resonance that occurs between the overtones of ν_4 and ν_6, and which causes the vibrational levels to be grouped into what looks like the vibrational angular momentum level structure of a degenerate vibration. As far as we are aware this type of pattern has not been seen before in the bending vibrations of an asymmetric top molecule. The combination of *a*- and *b*-axis Coriolis coupling with Darling–Dennison resonance distorts the spectra very severely. The *K*-structure is totally disorganized, and local rotational perturbations occur in the *J*-structure at many places where appropriate sets of levels happen to lie close to each other. For $K>0$ all the members of an overtone polyad appear in the spectra, whatever their nominal vibrational symmetries. Specifically, the distinction between *a* and *b* irreducible representations is lost, although *g*-*u* symmetry remains valid.

II. EXPERIMENTAL DETAILS

The *c*-axis polarization of the $\tilde{A}-\tilde{X}$ transition implies the rotational selection rule $K'-\ell''=\pm 1$. Taking account of the *g*-*u* symmetry properties of the levels, it has been necessary to carry out four sets of experiments in order to map the $K'=0-2$ structure of the $\tilde{A}$ state, as illustrated in Fig. 1. In one-photon jet-cooled experiments from the ground vibrational level, which has $\ell''=0$, only the vibrationally gerade $K'=1$ levels are accessible in the absence of Coriolis- or axis-switching-induced "forbidden" subbands. To get at the gerade $K'=0$ and 2 levels, it is necessary to use a warmed

sample that has a sufficient population in the ground state ν_4 fundamental, where $\ell''=1$. Similarly, for the ungerade vibrational levels, observed in IR-UV double resonance experiments, only the ungerade $K'=1$ levels can be reached if the intermediate level is a Σ^+_u ($\ell''=0$) ground state vibrational level, such as the ν_3 fundamental; a Π_u vibrational intermediate ($\ell''=1$) is needed in order to reach the ungerade $K'=0$ and 2 levels.

Laser-induced fluorescence spectra of neat acetylene have been recorded in an unskimmed pulsed jet expansion. The gas was expanded through a pulsed valve (General Valve, Series 9) with a 0.5 mm orifice from a backing pressure of 200 kPa. The ultimate vacuum achieved in the apparatus was 2.7×10^{-5} Pa, which rose to 6.7×10^{-3} Pa under normal gas load.

The laser radiation was the frequency-doubled output of a Lambda Physik 3002E dye laser, pumped by the third harmonic of a Nd:YAG laser (Spectra-Physics DCR-3). A small portion of the dye laser power was passed through a heated gas cell containing $^{130}Te_2$ vapor for calibration (±0.02 cm^{-1} accuracy), while the remainder was doubled in a β-barium borate crystal, and sent to the molecular beam chamber. The laser radiation crossed the pulsed jet about 3 cm from the orifice.

Fluorescence from the excited acetylene was observed at right angles to both the laser beam and the jet axis. The fluorescence was collected by a lens system and detected by a Hamamatsu R331 photomultiplier after passing through a UG-5 or UG-11 colored glass filter.

To observe the $K'=0$ and 2 levels belonging to gerade vibrational states it has been necessary to record hot band transitions from the ground state ν_4 fundamental. In order to induce hot bands in the jet spectra while maintaining reasonably low rotational temperatures, the distance between the nozzle and the intersection of the laser with the pulse of molecules was reduced from ~30 to ~5 mm. Additionally, the relative timing of the pulsed valve and the laser was adjusted so that the laser radiation intersects the leading edge of the gas pulse, which is characterized by higher effective vibrational temperatures.

The ungerade vibrational states have been observed by IR-UV double resonance, using the ν_3 and $\nu_3+\nu_4$ IR bands as intermediates. The infrared radiation was generated in a two-step difference frequency generation/optical parametric amplification process. A portion of the 1064 nm output of an injection-seeded Nd:YAG laser (Spectra-Physics PRO-270) was mixed, in a lithium niobate ($LiNbO_3$) crystal, with the output of a dye laser (Lambda Physik FL 2002) operating with either LDS 798 or LDS 751. The resulting infrared radiation was then passed through a second $LiNbO_3$ crystal, which was pumped by the remainder of the 1064 nm beam. The amplified IR radiation had an energy of approximately 3 mJ/pulse and a spectral width of 0.15 cm^{-1}, which is limited by the resolution of the grating-tuned dye laser.

A small fraction of the IR beam was sent to a photoacoustic cell containing 10 torr of acetylene gas. The observed photoacoustic signal was used to ensure that the IR frequency stayed in resonance with the desired vibrational transition. The remaining IR radiation entered the chamber through a CaF_2 window in the opposite direction to the UV laser. The relative timing of the two lasers was adjusted so that the beams were temporally overlapped, with the precise timing adjusted to maximize the observed double resonance fluorescence signals.

III. THEORY

The energy level pattern for the coupled ν_4 and ν_6 bending fundamentals of the $\tilde{A}\,^1A_u$ state of C_2H_2 has been described by Utz *et al.*[33] and is similar to that analyzed by Hegelund *et al.*[37] in the infrared spectrum of the *trans*-bent molecule diimide N_2H_2. The overtones of ν_4 and ν_6, which are the subject of the present work on C_2H_2, require, in addition, considerations of anharmonicity and Darling–Dennison resonance.[38] A summary of the relevant theory follows.

A. Matrix elements of the rotational and Coriolis operators

For an asymmetric top molecule such as C_2H_2 in its $\tilde{A}\,^1A_u$ state, the general rotational Hamiltonian[39–41] simplifies to

$$H_{\rm rot}=A(J_a-G_a)^2+B(J_b-G_b)^2+C(J_c-G_c)^2, \tag{1}$$

where A, B, and C are the rotational constants, J is the total angular momentum, G is the vibrational angular momentum, and a, b, and c refer to the principal inertial axes. When the squares are expanded, this equation becomes

$$H_{\rm rot}=AJ_a^2+BJ_b^2+CJ_c^2-2AJ_aG_a-2BJ_bG_b-2CJ_cG_c+AG_a^2+BG_b^2+CG_c^2. \tag{2}$$

The first three terms are the familiar rigid rotator Hamiltonian, followed by the three first-order Coriolis terms, and finally three terms involving the squares of the components of the vibrational angular momentum. These components are defined[42,43] as

$$G_\alpha=\mathbf{Q}^{\rm tr}\boldsymbol{\zeta}^\alpha\mathbf{P}, \tag{3}$$

where $\mathbf{Q}$ and $\mathbf{P}$ are the vectors of vibrational normal coordinates and their conjugate momenta, and $\boldsymbol{\zeta}^\alpha$ is a skew-symmetric matrix of Coriolis coupling constants. Multiplying this out, and considering just the vibrations ν_4 and ν_6,

$$G_\alpha=Q_4\zeta_{46}{}^\alpha P_6-Q_6\zeta_{46}{}^\alpha P_4. \tag{4}$$

For the $\tilde{A}\,^1A_u$ state of C_2H_2 the only nonvanishing coupling constants between the ν_4 and ν_6 vibrations are $\zeta_{46}{}^a$ and $\zeta_{46}{}^b$, which are related by the sum rule,[13,41]

$$(\zeta_{46}{}^a)^2+(\zeta_{46}{}^b)^2=1. \tag{5}$$

The terms in G_c can therefore be ignored, since there is no c-axis coupling.

The matrix elements of the vibrational angular momentum operators follow from the matrix elements of the Q and P operators in a harmonic basis,[40]

$$\langle v_4+1v_6|G_\alpha|v_4v_6+1\rangle = -i\zeta_{46}{}^{\alpha}\hbar\Omega[(v_4+1)(v_6+1)]^{1/2},$$
$$\langle v_4v_6+1|G_\alpha|v_4+1v_6\rangle = i\zeta_{46}{}^{\alpha}\hbar\Omega[(v_4+1)(v_6+1)]^{1/2}, \quad (6)$$

where Ω is Mills' abbreviation,[44]

$$\Omega = [(\nu_4/\nu_6)^{1/2} + (\nu_6/\nu_4)^{1/2}]/2. \quad (7)$$

Since the highest J values in either our jet-cooled spectra or our double resonance spectra are never more than 9, centrifugal distortion effects can be ignored. In a signed-k basis the matrix elements of the rigid rotator and first-order Coriolis terms are then

$$\langle v_4v_6Jk|H|v_4v_6Jk\rangle = \left[A - \tfrac{1}{2}(B+C)\right]k^2 + \tfrac{1}{2}(B+C)J(J+1),$$

$$\langle v_4v_6Jk \pm 2|H|v_4v_6Jk\rangle = \tfrac{1}{4}(B-C)[J(J+1) - k(k\pm 1)]^{1/2}[J(J+1) - (k\pm 1)(k\pm 2)]^{1/2},$$

$$\langle v_4+1v_6Jk|H|v_4v_6+1Jk\rangle = 2iA\zeta_{46}{}^{a}\Omega k[(v_4+1)(v_6+1)]^{1/2},$$

$$\langle v_4+1v_6Jk \pm 1|H|v_4v_6+1Jk\rangle = iB\zeta_{46}{}^{b}\Omega[J(J+1) - k(k\pm 1)]^{1/2}[(v_4+1)(v_6+1)]^{1/2},$$

$$\langle v_4v_6+1Jk|H|v_4+1v_6Jk\rangle = -2iA\zeta_{46}{}^{a}\Omega k[(v_4+1)(v_6+1)]^{1/2},$$

$$\langle v_4v_6+1Jk \pm 1|H|v_4+1v_6Jk\rangle = -iB\zeta_{46}{}^{b}\Omega[J(J+1) - k(k\pm 1)]^{1/2}[(v_4+1)(v_6+1)]^{1/2}. \quad (8)$$

The matrix elements of the terms in $G_\alpha{}^2$ can be obtained by matrix multiplication from Eq. (6). There are nine possible expressions, but the only important ones are the diagonal element and the elements that act within a given vibrational polyad, defining this as one where the levels have the same value of v_4+v_6,

$$\langle v_4v_6|AG_a{}^2 + BG_b{}^2|v_4v_6\rangle = [A(\zeta_{46}{}^{a})^2 + B(\zeta_{46}{}^{b})^2](2v_4v_6 + v_4 + v_6),$$

$$\langle v_4v_6|AG_a{}^2 + BG_b{}^2|v_4+2v_6-2\rangle = -[A(\zeta_{46}{}^{a})^2 + B(\zeta_{46}{}^{b})^2][(v_4+1)(v_4+2)v_6(v_6-1)]^{1/2},$$

$$\langle v_4v_6|AG_a{}^2 + BG_b{}^2|v_4-2v_6+2\rangle = -[A(\zeta_{46}{}^{a})^2 + B(\zeta_{46}{}^{b})^2][v_4(v_4-1)(v_6+1)(v_6+2)]^{1/2}. \quad (9)$$

In deriving these elements the factors of $\hbar^2$ are absorbed into the rotational constants, and Ω^2 has been taken as exactly 1; terms involving $[(\nu_4/\nu_6)^{1/2} - (\nu_6/\nu_4)^{1/2}]^2$ were ignored since ν_4 and ν_6 are very nearly the same. The approximation of retaining only the matrix elements of $G_\alpha{}^2$ acting within a given polyad is not expected to cause problems, since the closest interacting polyads must differ by two units of v_4+v_6, as a result of the $g-u$ symmetry properties of the levels, and will be separated by about 1500 cm^{-1}.

It can be seen from the first line of Eq. (9) that one of the effects of the vibrational angular momentum is to add a quantity $[A(\zeta_{46}{}^{a})^2 + B(\zeta_{46}{}^{b})^2]$ to the vibrational frequencies ν_4 and ν_6. With the values of the parameters taken from the least squares analysis of the $v_4+v_6=2$ polyad, described below, this quantity is 7.06 cm^{-1}.

The vibrational angular momentum also adds twice this quantity, i.e., 14.12 cm^{-1}, to the anharmonicity parameter x_{46}. This is slightly larger than the observed value $x_{46} = 11.39$ cm^{-1} (described below), and implies that the anharmonic force field contributes a mere -2.73 cm^{-1} to x_{46}. The dominance of the angular momentum contribution to x_{46} is unusual and somewhat surprising. It also emphasizes that the role of vibrational angular momentum in generating what looks like anharmonicity should not be neglected.

B. Darling–Dennison resonance

The off-diagonal elements in Eq. (9) have the same vibrational quantum number dependence as those responsible for Darling–Dennison resonance.[38] This is a well-known effect[45–47] in the overtone spectroscopy of molecules such as H_2O and the ground state of C_2H_2. Provided that certain definite relationships between the Darling–Dennison resonance parameter and the anharmonicity constants are satisfied,[48] the Darling–Dennison resonance converts the normal mode energy level pattern of the low-lying stretching vibrational levels into a local mode pattern at higher energy.[45] This represents how the vibrational structure changes from the low energy pattern, where the two bonds vibrate in phase, to the high energy pattern approaching dissociation, where just one of the two bonds breaks. The strong Darling–Dennison resonance involving nearly degenerate bending vibrations in an asymmetric top appears to be a new phenomenon. Some aspects of the resulting vibrational level structure resemble what is found for stretching vibrations, but there are also differences; research into the various effects is continuing.

Darling–Dennison resonance has been considered in some detail by Lehmann.[49] He gives the matrix element as

$$\langle n_a+2n_b-2|H|n_an_b\rangle = \tfrac{1}{4}K_{aabb}[(n_a+1)(n_a+2)n_b(n_b-1)]^{1/2}, \quad (10)$$

where

$$K_{aabb} = \frac{1}{4}\phi_{aabb} + \sum_\alpha -B_\alpha(\zeta_{ab}{}^{\alpha})^2\frac{(\omega_a+\omega_b)^2}{\omega_a\omega_b} + \frac{1}{8}\sum_k \phi_{kaa}\phi_{kbb}\omega_k\left(\frac{1}{4\omega_a{}^2-\omega_k{}^2} + \frac{1}{4\omega_b{}^2-\omega_k{}^2}\right) - \frac{1}{2}\sum_k \phi_{kab}{}^2\frac{\omega_k}{\omega_k{}^2-(\omega_a-\omega_b)^2}. \quad (11)$$

Although the notation is different, the term involving the $\zeta_{ab}{}^{\alpha}$ parameters in Eq. (11) corresponds exactly to the coef-

ficient in the off-diagonal elements of Eq. (9). Allowing for the factor $\frac{1}{4}$ in Eq. (10), this term contributes an amount $-4[A(\zeta_{46}^{a})^2+B(\zeta_{46}^{b})^2]=-28.24$ cm^{-1} to the parameter K_{4466}. Again this is a surprisingly large amount, which (as shown below) outweighs the effects of the cubic and quartic anharmonic potential constants ϕ. It is remarkable that the vibrational angular momentum should make such a large contribution to what is usually thought of as anharmonicity, both for the x_{46} and K_{4466} parameters.

C. Structures of the Hamiltonian matrices

A complication in using the elements of Eq. (8) for a matrix calculation of the energy levels is that the first-order Coriolis terms are imaginary. This can be overcome by multiplying the $|v_6\rangle$ harmonic oscillator basis functions by a phase factor $(i)^{v_6}$. To implement this, the Hamiltonian matrices for each J-value from Eq. (8) are subjected to a similarity transformation, $\mathbf{H}'=\mathbf{S}^{\dagger}\mathbf{H}\mathbf{S}$. The $\mathbf{S}$ matrix consists of blocks for each vibrational level that take the sums and differences of the signed-k basis functions, converting them to an unsigned-K basis,[50] but with all the elements in the blocks for the various vibrational levels multiplied by $(i)^{v_6}$. The transformation factorizes the matrix for each J-value into two submatrices, which can be given e and f symmetry labels. Further factorization is not possible because of the $\Delta K=\pm 1$ form of the b-axis Coriolis elements.

After the transformation the matrix elements are all real, but any element off-diagonal in the vibrational quantum numbers carries a negative sign. The energy matrices can then be constructed directly from Eqs. (8) and (10), taking account of the signs and the vibrational symmetries. Writing the basis functions as $|K^{\pm}x\rangle$, where $\pm$ indicates sum or difference and x is the irreducible representation label a or b, the e matrix contains the functions $|0^+a\rangle,|1^-a\rangle,|1^+b\rangle,|2^+a\rangle,|2^-b\rangle,|3^-a\rangle,\ldots$, while the f matrix has the same structure but with the a and b labels reversed. As is well known,[50] the $\langle k=-1|H|k=1\rangle$ asymmetry element is added to or subtracted from the $|K=1\rangle$ diagonal element by the similarity transformation, and any element connecting a $|k=0\rangle$ basis function to a $|k=\pm 1\rangle$ or $|k=\pm 2\rangle$ basis function gets multiplied by $2^{1/2}$.

D. Selection rules. Coriolis coupling and axis-switching

In the absence of Coriolis and axis-switching[16] effects, the rotational selection rules for the c-axis polarized $\tilde{A}\,^1A_u-\tilde{X}\,^1\Sigma^+_g$ transition are $K'-\ell''=\pm 1$, $\Delta J=0,\pm 1$. Both Coriolis and axis-switching effects act to destroy the strictness of the first rule, giving rise to additional $K'-\ell''=0,\pm 2$ subbands. Because of this it is difficult to distinguish the two effects, and, in fact, it is possible to rationalize axis-switching effects using the formalism of Coriolis coupling.[15,51,52] In this paper the term axis-switching will be used to describe the forbidden subbands of the Franck–Condon allowed 3^n and 2^13^n progressions. These are easily recognized since the K-structures of the upper levels follow the normal asymmetric top energy level expressions, because there is no competing Coriolis coupling. The forbidden subbands in the bending polyads are best described as Coriolis-induced since this is the principal mechanism for their appearance. These forbidden subbands are mostly fairly weak but a few are surprisingly strong, particularly when two sets of levels with zero-order K values differing by one unit happen to lie close to each other.

As for the vibrational selection rules, these are found to be obeyed strictly only for the $K=0$ levels of the v_4+v_6 =even polyads, where $K'=0$ levels with b_g vibrational symmetry are not seen. For the v_4+v_6=odd polyads, the $K'=0$ levels with both a_u and b_u vibrational symmetry appear in double resonance spectra via Π_u intermediate levels ($\ell''=1$). They can be distinguished by their different rotational selection rules. For instance, in transitions from f-symmetry rotational levels of a Π_u intermediate level, $K'=0$ levels with a_u vibrational symmetry (which have e rotational symmetry) give only Q branches, while those with b_u vibrational symmetry (f rotational symmetry) give R and P branches; the pattern is reversed in transitions from e-symmetry intermediate levels. The relative strengths of double resonance transitions to $K'=0$ levels with a_u and b_u vibrational symmetry are found to depend on which Π_u intermediate state is chosen. Transitions to b_u levels dominate when $\nu_3+\nu_4$ is used as the intermediate, though experiments with other polyads have shown that transitions to a_u levels dominate when $\nu_1+\nu_5$ is used as the intermediate. It is not clear why this should be so. For $K\neq 0$ levels the a-axis Coriolis mixing is so strong that every vibrational level appears in the spectrum, with the only restriction being that $K'-\ell''=\pm 1$ transitions are usually the most intense.

For simplicity in what follows the distinction between K for the $\tilde{A}\,^1A_u$ state and ℓ for the $\tilde{X}\,^1\Sigma^+_g$ state will not always be made. The two quantities describe the projection of the total angular momentum along the linear or near-linear inertial axis, and are essentially equivalent.

IV. RESULTS

The structures of the bending polyads are highly irregular because of the interplay of the Coriolis coupling and the Darling–Dennison resonance. Both of these are very large effects, with the experimental Darling–Dennison parameter K_{4466} found to be about -50 cm^{-1}, and the Coriolis parameter $2A\zeta^a$ (which is the coefficient of K in the a-axis coupling elements) about 18 cm^{-1}. It is not possible to separate them, or to understand the structures of the polyads, without data from levels with several K-values. For instance, it is essential to have data from as many of the $K=0$ stacks as possible, because these contain no a-axis Coriolis effects, and allow the vibrational origins to be established. Even so, these vibrational origins are not the fully deperturbed origins, because they represent the levels that result after the Darling–Dennison resonance has acted between harmonic basis levels of the same symmetry. The higher-K stacks suffer from both Darling–Dennison and Coriolis effects, but the effects can be separated because the a-axis Coriolis coupling depends linearly on K, whereas the Darling–Dennison resonance is independent of K. This means that a successful least squares analysis of a bending polyad requires data from

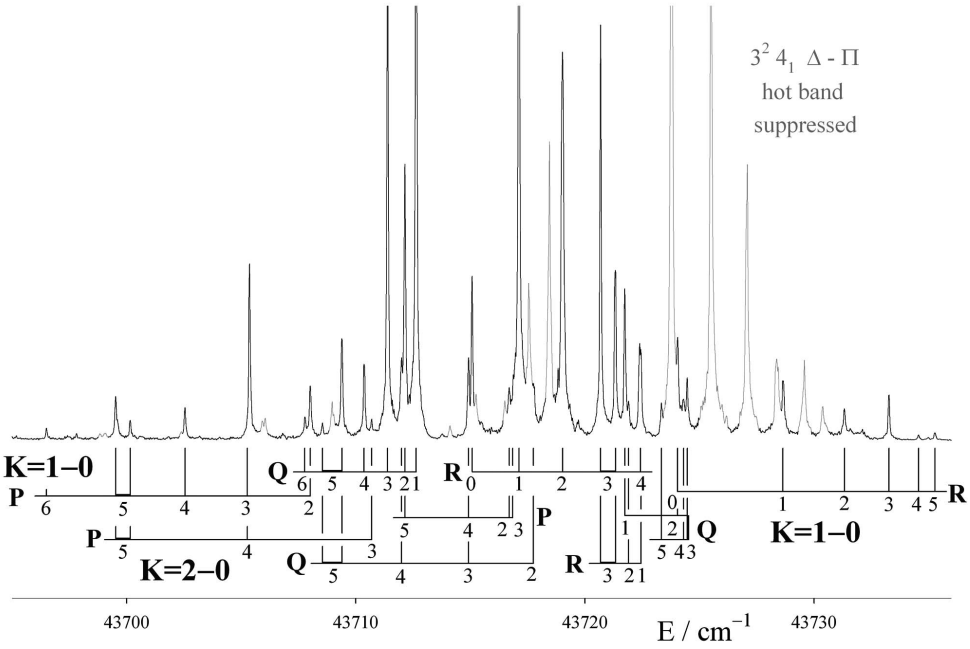

FIG. 2. Low frequency part of the $\upsilon_4+\upsilon_6=2$ (B^2) polyad of the $\tilde{A}\,^1A_u$ state of C_2H_2, observed in one-photon laser excitation. Three subbands are present, representing three interacting K-stacks, two with $K'=1$ and one with $K'=2$. The lines of an overlapping hot band (3^24_1,Δ-Π) have been colored gray.

$K=0$, 1, and 2 stacks, at the minimum. It is of course necessary to use the deperturbed band origins in order to calculate the higher-K levels correctly, since the Coriolis coupling and the Darling–Dennison resonance are both perturbations on the rigid rotator-harmonic oscillator basis.

A. The $v_4+v_6=2$ polyad (B^2)

The first overtone polyad ($\upsilon_4+\upsilon_6=2$, or B^2, where B means "bending") lies near 43 700 cm^{-1}. It consists of three vibrational levels: 4^2, 4^16^1, and 6^2. In room temperature absorption spectra it is completely buried under very intense hot band structure from the Franck–Condon allowed 3^24_1 band, but in jet-cooled LIF experiments the hot bands are sufficiently reduced to make analysis possible. Two regions of structure can be recognized: a confused group of lines centered at 43 715 cm^{-1} and an elegantly simple $K'-\ell''=1-0$ subband at 43 796 cm^{-1}. The 43 715 cm^{-1} group is illustrated in Fig. 2. In this figure the lines of an overlapping hot band have been coloured light gray.

The bands shown in Fig. 2 represent transitions from the ground vibrational level of the molecule to the lower two of the three $K'=1$ levels of the polyad, together with a Coriolis-induced $K=2-0$ subband. One of the $K=1-0$ subbands, with Q head at 43 712 cm^{-1}, is easily assigned, and accounts for most of the strong lines. Somewhat surprisingly for a level so low in the vibrational manifold, it contains perturbations at $J'=4e$ and $5f$. Because of the unexpectedly large Coriolis perturbations and the severe blending, the remaining structure could not be assigned until the $\upsilon_4+\upsilon_6=3$ (B^3) polyad had been analyzed, and the Darling–Dennison resonance recognized. Calculations of the rotational structure then allowed the remaining lines, and the perturbations, to be assigned immediately.

Experiments with a warmed beam gave the spectrum shown in Fig. 3. The energy range illustrated lies below that of Fig. 2 by the amount of the ground state ν_4 fundamental, and shows four of the $K'=0$ and 2 stacks as hot bands from ν_4''. The $K'=0$ subbands belong to the two overtones, namely 4^2 and 6^2, which have a_g vibrational symmetry. Although the ν_4 and ν_6 fundamentals lie only 3 cm^{-1} apart, the two overtones are 52 cm^{-1} apart, as a result of the Darling–Dennison resonance. The third $K'=0$ hot band, going to the combination level 4^16^1 (b_g vibrational symmetry), is not seen. It would be observable if it lay close enough to one of the $K'=1$ levels to obtain some intensity by b-axis Coriolis coupling, but such is not the case here. It is calculated to lie at 43 131 cm^{-1}.

The $K'=1$ and 2 subbands near 43 110 cm^{-1} in Fig. 3 are hot bands with the same upper states as the cold bands near 43 720 cm^{-1} in Fig. 2. In Fig. 2 the intensity is carried by the $K'=1$ level, with the $K'=2$ level getting its intensity by b-axis Coriolis coupling; in Fig. 3 the roles of the two levels are reversed. Consistent with the line strengths for a $K=2-1$ band, the P branches of both bands are expected to be much weaker than the rest of the structure, and are not seen. The intense $K=2-1$ hot band at 43 138 cm^{-1} in Fig. 3 goes to the middle $K'=2$ level. The uppermost $K=2-1$ hot band is calculated to lie at 43 258 cm^{-1}, exactly at the position of the strong Franck–Condon allowed 3^1_0 band. It will be totally buried, and has not been searched for.

The assignments of the $K'=0$ and 2 hot bands near 43 140 cm^{-1} are confirmed by the observation of some very weak lines near 43 750 cm^{-1} in the cold spectra, corresponding to Coriolis-induced $K=0$-0 and 2-0 cold bands. These had been noted during the analysis of the cold spectra, but could not be assigned initially. The line assignments of the

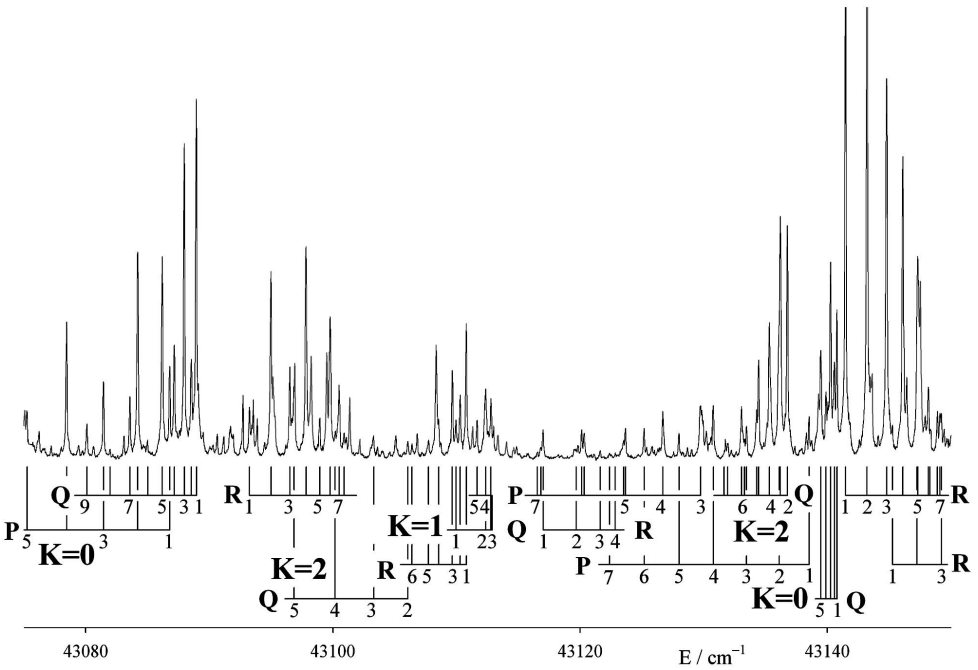

FIG. 3. Hot bands of the $v_4+v_6=2$ (B^2) polyad of the $\tilde{A}\,^1A_u$ state of C_2H_2; the region shown lies to the red of that shown in Fig. 2 by the amount of the ground state ν_4'' fundamental (π_g, 612 cm^{-1}). Overlapping lines from bands with $\nu_4''=2$ have been colored gray.

various subbands are given in Table I. In this table the subbands are labeled for convenience by Roman numerals in order of increasing energy for each K value.

The level structure of the B^2 polyad is illustrated in Fig. 4. The left hand side [Fig. 4(a)] shows the K-structure. The two overtones 4^2 and 6^2 are almost degenerate in zero-order, with 4^2 lying 2.1 cm^{-1} above 6^2; however, as a result of the Darling–Dennison resonance, they give rise to two well-separated $K=0$ levels, whose wave functions are very nearly the normalized sum and difference of $|4^2\rangle^{(0)}$ and $|6^2\rangle^{(0)}$. The $K=0$ level of 4^16^1 lies above the mid-point of the two overtones because of the x_{46} term. For $K=1$ the a-axis Coriolis coupling complicates the picture. The 4^16^1 level interacts essentially only with the upper of the mixed overtone levels, whose approximate wave function is the sum function $(2)^{-1/2}[|4^2\rangle^{(0)}+|6^2\rangle^{(0)}]$. The lower mixed overtone (difference function) is almost unaffected. The result is that the two upper $K=1$ levels are pushed apart, with one of them dropping almost to the energy of the lower mixed overtone. For $K\geqslant 2$ the Coriolis coupling between the upper mixed overtone and 4^16^1 is so large that the Coriolis-coupled levels become the top and bottom levels with their K-value. It is possible to view these effects as an interference between the Coriolis and Darling–Dennison interactions, which allows the sign of the Darling–Dennison parameter to be determined.

Figure 4(b) shows the observed and calculated J-structure plotted against $J(J+1)$. Only the low energy levels are illustrated, so that the highest observed $K=1$ level lies off the top of the figure. The most obvious irregularity is the very strong b-axis Coriolis perturbation between the lowest $K=2$ level and the second $K=1$ level. The two levels are almost exactly degenerate in zero-order, such that the splitting between them rises to over 20 cm^{-1} at $J=7$. The lower level, nominally $K=2$, is pushed down so hard that the R branch going to it (see Fig. 2) degrades entirely to the red, in contrast to the usual pattern. This level also cuts through the lowest $K=1$ level, causing the small perturbations mentioned at the beginning of this section.

An unexpected feature in Fig. 4(b) is the presence of an unseen $K=3$ level between the two uppermost $K=0$ levels. It appears not to perturb the nearby $K=2$ level, despite the possibility of b-axis Coriolis coupling (following $\Delta K=\pm 1$ selection rules), but to interact strongly with the two $K=0$ levels. Detailed examination of the rotational energy matrices and their eigenvectors confirms that the $K=2$ and $K=3$ levels should not interact. The vibrational wave functions for these levels are, to good approximation,

$$\begin{aligned} K=2:&\quad (2)^{-1/2}[|4^2\rangle^{(0)}-|6^2\rangle^{(0)}],\\ K=3:&\quad (2)^{-1/2}|4^16^1\rangle^{(0)}+(1/2)[|4^2\rangle^{(0)}+|6^2\rangle^{(0)}]. \end{aligned} \tag{12}$$

The b-axis Coriolis coupling between them would involve the matrix element

$$\langle 4^16^1|^{(0)}G_b[|4^2\rangle^{(0)}-|6^2\rangle^{(0)}], \tag{13}$$

where the two terms cancel exactly, to give zero. On the other hand, the $\Delta K=\pm 3$ interactions between the $K=3$ level and the two $K=0$ levels arise from vibrationally allowed cross-terms between the asymmetry and the b-axis Coriolis coupling.

With seven of the nine K-stacks with $K=0-2$ assigned, there are enough data for a least squares fit to the upper state term values. A simple model was chosen for the rotational structure. The rotational constants A, $\frac{1}{2}(B+C)$, and $B-C$ were varied just for the overtones 4^2 and 6^2, and it was assumed that the rotational constants for the combination

TABLE I. Assigned rotational lines of the pure bending polyads of the $\tilde{A}\,^1A_u$ state of C_2H_2. The members of the upper state polyads are labeled with Roman numerals in order of increasing energy for each K-value. Blended lines are marked with an asterisk ($*$).

(a) The $v_4+v_6=2(B^2)$ polyad

	I: K=0-1			III: K=0-1			III: K=0-0
J	R	Q	P	R	Q	P	Q
1	43 096.26	43 088.97	43 086.81	43 145.27	43 140.78	43 138.53	43 752.43
2	95.00	88.56	84.22	47.32*	40.58	36.04	
3	96.53	87.99	81.45	49.23	40.27	33.46	51.93
4	97.83	87.17	78.47	51.14	39.89_5	30.78	
5	98.95	86.20	75.25	53.05	39.47*	28.01	51.13_5
6	99.78	85.02		54.93*		25.19	
7	43 100.50*	83.59			38.74	22.38	
8	00.91	81.98		58.77		19.56*	
9		80.11					

	I: K=1-0			II: K=1-0			II: K=1-1		
J	R	Q	P	R	Q	P	R	Q	P
0	43 715.08			43 724.05					
1	17.13	43 712.64		28.64	43 721.75		43 117.01	43 109.96*	
2	19.03*	12.15	43 708.02	31.33	24.05*	43 716.70*	19.68?	12.36*	
3	20.69	11.39	05.37	33.27_3	24.47	16.8*	21.63	12.79	43 105.10*
4	22.40*	10.36_3	02.55_3	34.56	24.31		22.85	12.79?	
5	23.78*	09.40	43 699.53	35.28	23.34	12.15*		11.68	
6		07.78	96.50						
7			93.19						

	III: K=1-0			I: K=2-0			I: K=2-1		
J	R	Q	P	R	Q	P	R	Q	P
0	43 798.89								
1	43 800.94	43 796.51		43 722.45			43 110.80		
2	02.82	96.16	43 791.83	21.91	43 717.76		10.30	43 106.06*	
3	04.57_5	95.66	89.17	21.34	14.93	43 7107.70	09.66	03.30	43 098.95*
4	06.15	94.95_5	86.36		08.55	00.16	08.72ee	00.19ef	
5	07.59	94.10	83.385				07.73ee	43 096.85*fe	
6	08.90	93.08	80.26				06.40ff		
7	10.06	91.83*	77.00						
8		90.49							

TABLE I. (*Continued.*)

	II: K=2-0			II: K=2-1					
J	R	Q	P	R_{ee}	R_{ff}	Q_{ef}	Q_{fe}	P_{ee}	P_{ff}
1	43 753.15$_5$			43 141.48					
2	54.91$_5$	43 748.44		43.21		43 136.77			
3	56.48	47.84$_5$	43 741.39	44.80		36.20$_5$		43 129.75	
4	57.82	47.04$_5$	38.43	46.11		35.31	35.41	26.69	
5	59.00	46.08	35.28*	47.32*		34.29	34.44	23.68	23.53
6	60.01			48.30*	48.18	33.06	33.29	20.33?	20.13
7	60.72			49.12	48.91*		31.93	16.82	16.54
8						29.96			

(b) The $v_4+v_6=3$ (B^3) polyad

Line frequencies, as observed in double resonance via the Q branch of the $\nu_3+\nu_4$ IR band (3897.16 cm^{-1})

	I, K=0 (b_u)−1		II, K=0 (a_u)−1	III, K-0 (b_u)−1		IV, K=0 (a_u)−1	I, K=1-1		
J	R_{ff}	P_{ff}	Q_{ef}	R_{ff}	P_{ff}	Q_{ef}	R_{ff}	Q_{ef}	P_{ff}
1	44 454.11	44 446.65?	44 457.14	44 451.43		44 547.68	44 449.86	44 446.45	
2	56.24	44.63*	56.90	53.47	44 542.24	47.46	50.85	45.73	44 441.50
3	58.03	42.30	56.49	55.47	39.64	47.14	51.58	44.63*	38.08
4	59.55	39.72	55.82	57.37	37.01*		51.98	43.26	34.34
5	60.76*	36.91	54.92	59.18	34.32	46.23	52.26	41.61	30.36
6	61.57			61.00	31.47				26.13
7	62.11*			62.77	28.63				
8					25.69				

	II, K=1-1			III, K=1-1			IV, K=1-1		
J	R_{ff}	Q_{ef}	P_{ee}	R_{ff}	Q_{ef}	Q_{fe}	R_{ff}	Q_{ef}	P_{ff}
1	44 484.48	44 481.18*		44 511.42	44 506.73*		44 618.13	44 613.73	
2		79.77*	76.62	13.72	06.73*	44 506.73			
3		81.18*		15.78	06.73*				44 606.36
4		79.77*		18.92	06.48*				
5	R_{ee}(2)	78.53	Q_{fe}(2)	20.53	07.19	R_{ee}(2)			
6	88.22		79.85		06.48*	13.76			

	I, K=2-1			II, K=2-1			III, K=2-1		
J	R_{ff}	Q_{ef}	R_{ee}	R_{ff}	Q_{ef}	P_{ff}	R_{ff}	Q_{ef}	P_{ff}
1	44 469.14			44 487.76			44 545.17		
2	70.97	44 464.46	44 470.99	83.32	44 483.05		47.01	44 540.51	
3	72.51	63.93		81.52	76.21	44 476.03	48.65	39.94	44 533.43
4	73.65	63.18		79.77*	72.10	66.85	50.06	39.23	30.55

TABLE I. (*Continued.*)

	I, K=2-1			II, K=2-1			III, K=2-1		
J	R_{ff}	Q_{ef}	R_{ee}	R_{ff}	Q_{ef}	P_{ff}	R_{ff}	Q_{ef}	P_{ff}
5	73.94	62.10*		79.06	67.93		51.24	38.30	27.43
6							52.28	37.21	24.17
7							53.07	35.94	20.65
8			$Q_{fe}(2)$			$Q_{fe}(2)$		34.49	
9			64.43			83.11		32.82	

	IV, K=2-1			I, K=3-1			II, K=3-1		
J	R_{ff}	Q_{ef}	P_{ee}	R_{ff}	Q_{ef}	P_{ff}	R_{ff}	Q_{ef}	R_{ee}
1	44 707.97								
2	09.82	44 703.26		44 497.06			44 515.18		44 415.23
3	11.46	02.75	44 696.23	99.12	44 489.99		17.04*	44 508.12	
4	12.95	02.05	93.33	44 500.32	89.71	44 480.57	17.04*	07.63	
5	14.30	01.21	90.29	00.89	88.50	77.95	18.13	05.28	
6	15.46	00.22		01.10	86.70			04.07	
7	16.46	44 699.01						02.65?	

Upper state term values, observed in IR-UV double resonance via the ground state ν_3 fundamental, (grating scans, where the calibration is less accurate).

J	I, K=0f	II, K=0e	III, K=0f	IV, K=0e	I, K=1e	I, K=1f	II, K=1e	II, K=1f
1	44 451.64	44 459.37		44 549.98	44 448.90	44 448.57	44 483.55	44 483.61
2	56.44	64.01		54.51	52.72	52.22	86.67	86.82
3	63.26	70.58		61.30	58.72	57.86	95.20	95.34
4	72.18	79.31	44 569.55	70.22	66.79	65.65	44 503.42	44 503.63
5	83.08	90.21	80.81	81.53	76.82	75.43	13.72	14.14
6	95.98	44 503.41*	94.47		89.07	87.53	26.18	26.72
7		17.72?			44 503.37?		40.52	

J	III, K=1e	III, K=1f	IV, K=1e	IV, K=1f	I, K=2e	I, K=2f	II, K=3e	II, K=3f
1	44 509.03	44 508.99	44 616.01	44 616.07				
2	13.80	13.63	20.52	20.32	444 71.49	44 471.49		
3	20.67	20.65	27.05	27.14	77.90	77.97		44 52.21?
4	29.95	29.83	35.93	35.84	86.58	86.53	44 431.23?	31.09
5	42.47	42.41	46.93	46.92	97.43	97.21	40.99	40.89
6	55.93	55.72	60.14	60.23	44 509.61	44 509.11	54.04	53.33
7	71.18		75.56		22.60		69.09	

II, K=2, J=2e: 44 490.16; J=2f: 44 490.21

TABLE I. (*Continued.*)

(c) The $v_4+v_6=4$ polyad (B^4); line frequencies in one-photon LIF

	I, K=0-1			I, K=1-0			II, K=1-0			V, K=1-0	
J	R	Q	P	R	Q	P	R	Q	P	R	Q
0				45 184.05			45 201.52			44 448.21	
1	44 564.97	44 560.66	44 558.50*	85.77	45 181.69		03.83	45 199.12*		50.33	45 445.84
2	66.60	60.27	55.92	87.10	80.90	45 177.02	05.71	99.12*	45 194.47	52.22	45.54
3	68.08	59.58	53.14	88.02	79.77	73.99	07.14	99.28	92.05	53.98	45.11
4	69.27	58.74*	50.08	88.56*	78.25	70.62	08.14	99.46*	89.24	55.60	44.53
5		57.64	46.97*	88.56*	76.33	66.86	08.70			57.10	43.76
6					73.99*						
7					71.25						

	I, K=2-0		II, K=2-0		II, K=2-1	
J	R	Q	R	Q	R	Q
1	45 196.97		45 226.47		44 614.83*	
2	97.65	45 192.26	28.45	45 221.80	16.79	44 610.14
3	98.20	90.52	30.36	21.38	18.69	09.73
4	98.68	88.56		20.81		09.14*
5		86.48		20.12		08.49
6						07.46?
7						06.35?

(d) The $v_4+v_6=5$ polyad (B^5); line frequencies in IR-UV double resonance via the 3897.16 cm^{-1} Q branch head

	V, K=0 (b_u)−1		VI, K=0 (a_u)−1	V, K=2-1	
J	R	P	Q	R	Q
1	46 195.09		46 190.90	46 173.88	
2	97.13	46 185.88	90.69	75.67	46 169.17
3	99.09	83.32	90.40	77.37	68.69
4	46 200.90	80.66	89.99	78.84	67.96
5	02.66	77.88	89.48	80.24	67.10
6		75.04			
7		72.08			

V, K=2-1, P(2): 46 162.10

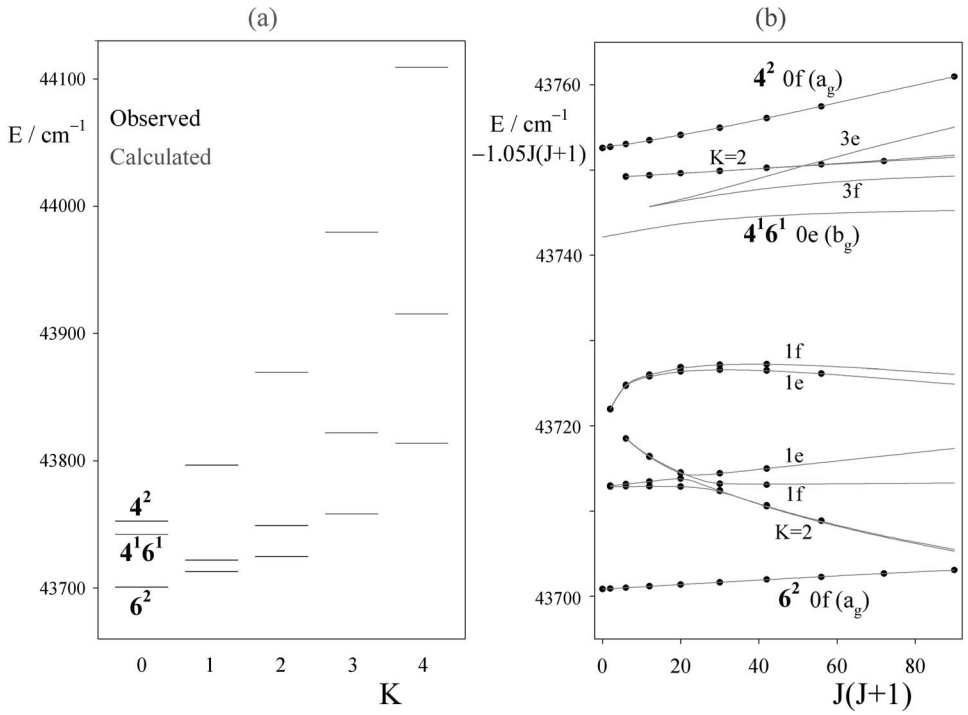

FIG. 4. (a) K-structure of the $v_4+v_6=2$ (B^2) polyad. Observed levels are shown in black, calculated levels in gray. (b) J-structure of the eight lowest K-stacks of the B^2 polyad, with observed levels shown as black dots, and calculated structure as gray lines. A quantity 1.05 $J(J+1)$ has been subtracted in order to expand the scale.

level $4^1 6^1$ were the averages of those for the two overtones. For the coupling terms, the two Coriolis parameters $2A\zeta^a$ and $B\zeta^b$ and the Darling–Dennison parameter K_{4466} were varied initially, though it was later found that adding a centrifugal distortion correction to K_{4466} improved the fit considerably. This was taken as

$$K_{4466}^{\text{eff}} = K_{4466}^{(0)} + K_{4466,D}K^2. \tag{14}$$

The vibrational parameters required some care. Since the $K'=0$ stack of the combination level $4^1 6^1$ is not seen, there are only two observable band origins, corresponding to the overtones 4^2 and 6^2, heavily mixed by the Darling–Dennison interaction. In the end it was decided to include the $J=K=0$ energies of the two fundamentals ν_4 and ν_6 (from the work of Utz *et al.*[33]), and to adjust, by least squares, ω_4, ω_6, and two of the three anharmonicity parameters x_{44}, x_{46}, and x_{66}. The value of x_{66} was then fixed at -4.22_6 cm^{-1}, as obtained from combining the position of the ν_6 fundamental with the deperturbed origin of the 6^3 overtone [described in Sec. IV B]. The fit is extremely good, with an rms error of 0.011 cm^{-1}, which is comparable to the accuracy of the line measurements; the results are given in Table II.

The most surprising result is the large size of the parameters x_{46} and K_{4466}. These are made up of contributions from the vibrational angular momentum and the anharmonic force field, and in both cases the vibrational angular momentum contribution is the larger. It is interesting to compare the anharmonic contributions with those calculated from the anharmonic force field of Ref. 36. For the Darling–Dennison parameter K_{4466}, where the experimental value, −51.68 cm^{-1}, includes −28.24 cm^{-1} from the vibrational angular momentum (meaning that the anharmonic contribution is −23.44 cm^{-1}) a calculation using Eq. (11) gives −16.6 cm^{-1}.

TABLE II. Rotational constants from least squares fitting of the B^2 polyad of the $\tilde{A}\ ^1A_u$ state of C_2H_2. Values are in cm^{-1}. The $J=K=0$ levels lie at 43 700.85 cm^{-1} (6^2, 1503.28 cm^{-1} above T_{00}), 43 742.13 ($4^1 6^1$, 1544.56) and 43 752.57 (4^2, 1555.00). Derived Coriolis constants: $\zeta^a=0.703_8$, $\zeta_b=0.711_1$; $(\zeta^a)^2+(\zeta^b)^2=1.001$. The only correlation coefficients with magnitudes over 0.9 are $\frac{1}{2}(B+C)$ $(6^2)/\frac{1}{2}(B+C)$ (4^2) −0.996, $A(6^2)/A$ (4^2) −0.981, and ω_4/x_{44} −0.949.

ω_6	772.497	±	0.032	A (6^2)	13.356	±	0.128
ω_4	764.709		0.075	$\frac{1}{2}(B+C)$ (6^2)	1.0806		0.0077
x_{66}	−4.226		fixed	$(B-C)$ (6^2)	0.1262		0.0077
x_{46}	11.385		0.080	A (4^2)	12.857		0.138
x_{44}	0.191		0.047	$\frac{1}{2}(B+C)$ (4^2)	1.0743		0.0080
$2A\zeta^a$	18.449		0.005	$(B-C)$ (4^2)	0.0530		0.0088
$B\zeta^b$	0.7980		0.0023	$K_{4466,D}$	0.0381		0.0281
K_{4466}	−51.678		0.020				
			rms error=0.0112 cm^{-1}				

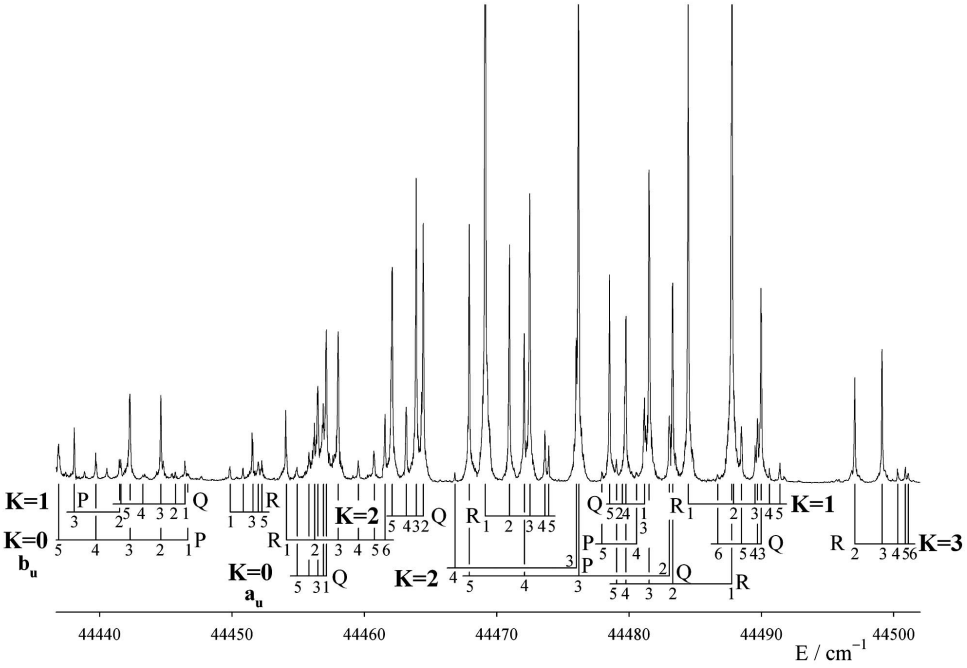

FIG. 5. Low energy part of the $v_4+v_6=3$ (B^3) polyad of the $\tilde{A}\,^1A_u$ state of C_2H_2, as observed in IR-UV double resonance via the $Q(1)-Q(5)$ lines of the ground state $\nu_3+\nu_4$ combination band (3897.16 cm^{-1}).

Similarly, for x_{46}, where the anharmonic contribution is -2.73 cm^{-1}, a calculation using the symmetry-allowed terms from Mills' perturbation theory expression,[53]

$$x_{46}=\tfrac{1}{4}\phi_{4466}-\tfrac{1}{4}\sum_k \phi_{44k}\phi_{k66}/\omega_k \tag{15}$$

gives $+1.08$ cm^{-1}. At the same time the experimental anharmonicity parameters x_{44} and x_{66} in Table II are quite small, which suggests that the pure bending motions are comparatively harmonic, once allowance is made for the vibrational angular momentum.

As for the Coriolis coupling parameters, these are almost unchanged from the values found in the fundamentals,[33] where $2A\zeta^a=18.47$ cm^{-1} and $B\zeta^b=0.787$ cm^{-1}. It is interesting to see how accurately the zeta sum rule [Eq. (5)] holds in the B^2 polyad. The derived values of $\zeta_{46}{}^a$ and $\zeta_{46}{}^b$ are given in Table II; the sum of their squares is 1.001, compared to the theoretical value of 1.

The variation in the A rotational constants with v_4 and v_6 appears to be much smaller for the overtones (Table II) than for the fundamentals,[33] where $A(4^1)=11.36(8)$ cm^{-1} and $A(6^1)=14.59(13)$ cm^{-1}. However, we note that the average of $A(4^1)$ and $A(6^1)$ is close to the value in the zero-point level, 13.057(5) cm^{-1}.[13] It is known from the N_2H_2 spectrum[37] that there is almost 100% correlation between the A constants of two strongly a-axis Coriolis-coupled levels, such that only their sum is well-determined; this may also be affecting the determinations for the C_2H_2 fundamentals. In the overtones the correlation is less severe because there are more vibrational levels to provide data.

An interesting minor point is that the (deperturbed) asymmetry parameter $B-C$ is much smaller in the 4^2 level than it is in the 6^2 level. This is consistent with the C_2H_2 molecule becoming nonplanar on average as the torsional vibration is excited. The rationale is as follows. Since the inertial b and c axes interchange when C_2H_2 is twisted from *trans*-bent to *cis*-bent, there must be a point near a twisting angle of 90° where it is accidentally a symmetric top, with $B-C=0$. Therefore excitation of the torsional vibration must reduce $B-C$. The prototype molecule for this effect is H_2S_2, which is 90° twisted and accidentally almost exactly a symmetric top.[50,54]

B. The $v_4+v_6=3$ polyad (B^3)

The B^3 polyad consists of four vibrational levels, 4^3, 4^26^1, 4^16^2 and 6^3; their symmetries are a_u, b_u, a_u, and b_u, respectively. Two spectra of the polyad have been recorded by IR-UV double resonance. In one, the ground state ν_3 fundamental ($\ell=0$) was used as the intermediate level in order to observe the $K'=1$ levels; in the other the $\nu_3+\nu_4$ combination level ($\ell=1$) was used to observe the $K'=0$ and 2 levels. Because of the strong b-axis Coriolis coupling, some of the K' levels appear in both spectra.

The low energy part of the polyad is illustrated in Fig. 5, as seen following IR pumping of the Q branch of the $\nu_3+\nu_4$ band at 3897.16 cm^{-1}. This branch is very compact, so that when the IR laser is tuned to its head the first five lines are excited simultaneously, populating the $J=1f-5f$ rotational levels. This allows the complete double resonance spectrum to be recorded in one scan, though it loses the state-selectivity of pumping individual rotational lines. Nevertheless the line assignments could be made straightforwardly, using lower state combination differences. To assist with the assignments a scan was also taken via the $P(3)$ line of the band, which populates the $J=2e$ levels. This was valu-

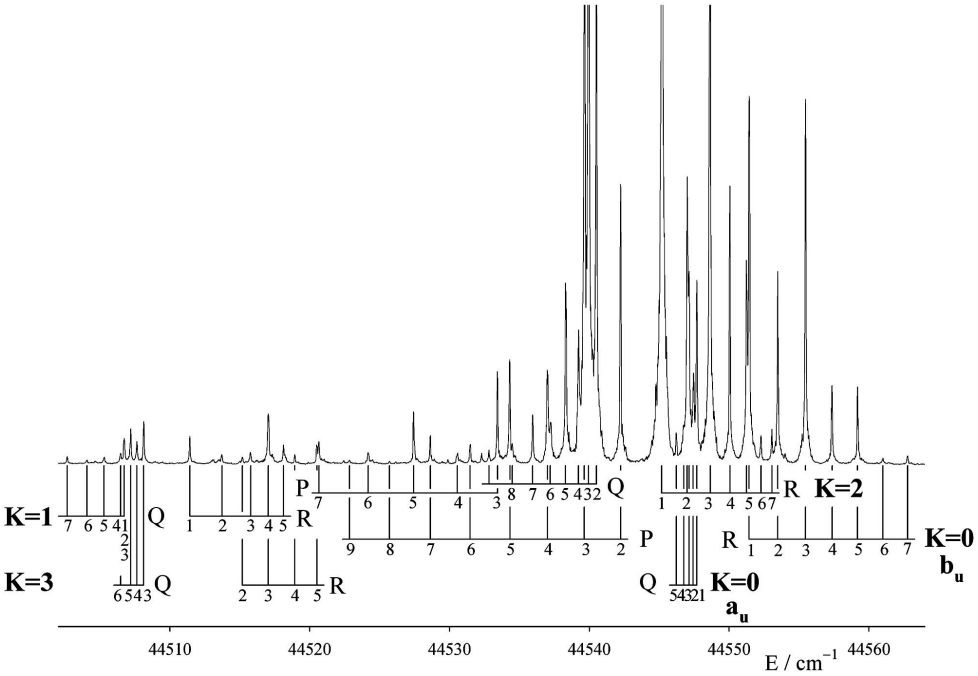

FIG. 6. Central part of the B^3 polyad; this spectrum is a continuation of Fig. 5 to higher energy. The two $K'=0$ subbands appear to be a single subband with R, Q, and P branches, but closer examination shows that the Q branch ($K=0$, a_u) is shifted up by 0.73 cm^{-1} relative to the R and P branches ($K=0$, b_u).

able in distinguishing the $K'=0$ subbands, since the branch structures depend on the parity of the intermediate levels, as described above.

The strongest features in Fig. 5 are two close-lying $K'=2$ subbands. The upper states interact with each other, and with nearby $K'=1$ and 3 levels, inducing extra subbands. At the low energy side are two $K'=0$ subbands separated by 8 cm^{-1}; they form a pair with b_u and a_u symmetries. There is also another weak Coriolis-induced $K'=1$ band.

The central part of the B^3 polyad is illustrated in Fig. 6. It contains the other two $K'=0$ subbands, again as a b_u/a_u pair, but this time separated by only 0.7 cm^{-1}. Also present are another strong $K'=2$ subband and weaker Coriolis-induced $K'=1$ and 3 bands. The remainder of the polyad, not illustrated, consists of a $K'=1$ subband at 44 614 cm^{-1} and a $K'=2$ subband at 44 703 cm^{-1}. These latter lie well above the rest of the polyad, and are not perturbed.

The K-and J-structures of the B^3 polyad are illustrated in Fig. 7. The left hand side [Fig. 7(a)] shows clearly how the Darling–Dennison resonance groups the four $K=0$ levels into two b_u/a_u pairs, separated by about 100 cm^{-1}. As expected from the near degeneracy of the ν_4 and ν_6 fundamentals, the four zero-order basis levels lie quite close to each other, with the overtones below the combinations by an amount $2x_{46}$. However, their separations are much smaller than the Darling–Dennison matrix element. The result is that one level of each symmetry is pushed up, and the other down, by the amount of the resonance matrix element, which in this case is 50 cm^{-1}. The patterns for higher K values are not so simple, though in first approximation the Coriolis coupling between the combination levels 4^16^2 and 4^26^1 pushes one of the levels far above the others.

The J-structure patterns [Fig. 7(b)] show a number of local avoided crossings caused by the b-axis coupling elements. These follow $\Delta K=\pm 1$ selection rules in the rigid rotator basis, and therefore act to destroy the goodness of K as a label. At the same time the Darling–Dennison resonance and the a-axis coupling, though diagonal in K, scramble the harmonic oscillator basis levels, so that the resulting patterns are often quite surprising. An example is given by the lowest two $K=2$ levels. The upper of these two, which begins near 44 480 cm^{-1}, is almost degenerate with the second $K=1$ level, and gets pushed down strongly by b-axis coupling with it. As in the B^2 polyad the R branch going to it degrades entirely to the red (see Fig. 5). At $J=6$ this $K=2$ level undergoes an avoided crossing with the lowest $K=2$, after which it goes on to perturb the two $K=0$ levels at the bottom of the pattern. Very clearly the K quantum number loses all meaning, as was noted also by Utz *et al.*[33] in their analysis of the fundamentals, though it is retained here as a convenient label. Another unexpected avoided crossing occurs between the $K=1$ and 3 levels near 44 510 cm^{-1}.

Fourteen K' stacks have been identified, representing all the stacks with $K=0-2$ together with two $K'=3$ stacks. This has allowed a detailed least squares treatment, of which the results are given in Table III. As might be expected from the density of perturbations, the main problem encountered was that of matching the eigenvalues of the Hamiltonian to the observed upper state term values. After some experimentation, the tactic adopted was to transform the Hamiltonian matrix in several steps. In the first step the Darling–Dennison resonance and the a-axis Coriolis coupling elements were diagonalized, after which the full Hamiltonian matrix was transformed by the resulting eigenvectors. Since the elements eliminated were diagonal in K, the transformed basis states preserved the values of K. In the second step the asym-

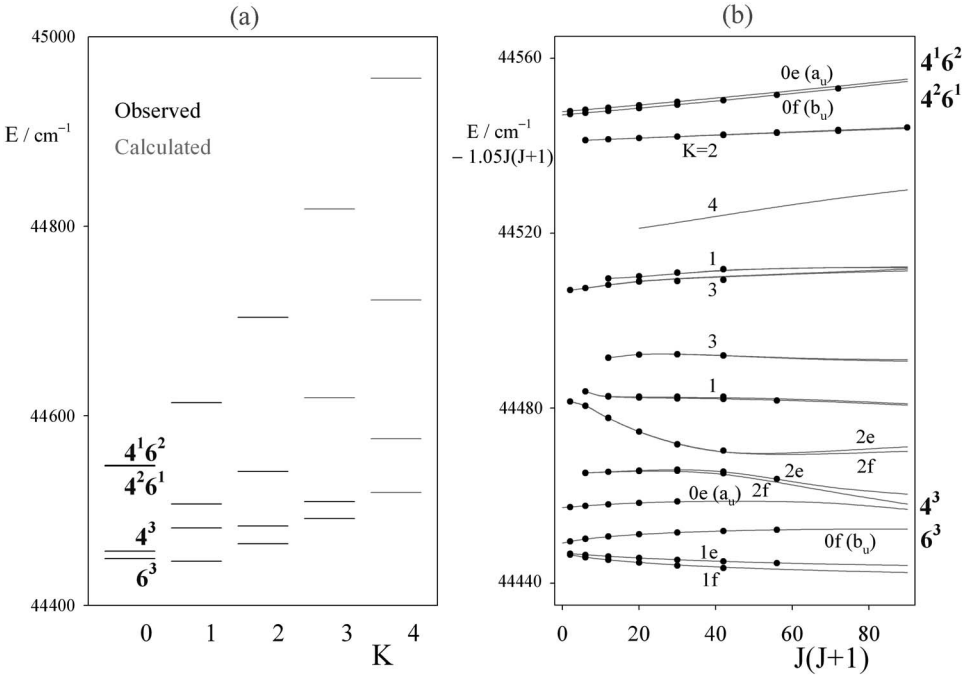

FIG. 7. (a) K-structure of the B^3 polyad of the $\tilde{A}\,^1A_u$ state of C_2H_2, with observed levels shown in black and calculated levels in gray. Vibrational assignments are marked for the $K=0$ levels, as given by their eigenvectors; for $K \geqslant 1$ levels the harmonic basis functions are so mixed that it is meaningless to give assignments. (b) J-structure of the 13 lowest energy K-stacks. Observed levels are shown as dots, calculated as gray lines. Two major avoided crossings occur: one between the $K=1$ and 3 levels near 44 510 cm^{-1} and the other involving the second $K=2$ level, which interacts with the lowest $K=2$ and the second $K=1$ levels.

metry elements ($\Delta K = \pm 2$) were diagonalized, such that the next set of transformed functions still retained the odd- or even-K character of the original basis functions. Finally the doubly transformed Hamiltonian matrix was diagonalized, eliminating the b-axis coupling, and the eigenvalues sorted according to their eigenvector coefficients. Even so, it was found that the sorting was not always accurate at the most severe of the avoided crossings, so that the stacks with a given nominal K-value were then placed in ascending order.

Again, a simple model was used for the rotational energy, where only the A, $\frac{1}{2}(B+C)$, and $B-C$ constants for the overtones 4^3 and 6^3 were varied, with those for the combinations being interpolated between those of the overtones. As in the B^2 polyad, the coupling terms used were K_{4466}, $2A\zeta^a$, and $B\zeta^b$, though the first two were allowed centrifugal distortion corrections as in Eq. (14). No attempt was made to write the band origins in terms of anharmonicity parameters, instead the four deperturbed origins were taken as adjustable parameters.

The final fit was not quite as good as that for the B^2 polyad, but there are other factors to consider. The first is the possibility of Fermi resonance between the B^3 polyad and the 2^1B^1 polyad, which lies about 100 cm^{-1} below. In fact, with the strong a-axis coupling in both polyads the K-structure of 2^1B^1 catches up rapidly to that of B^3, such that its upper $K=2$ level lies only 40 cm^{-1} below the lowest $K=2$ of B^3. An attempt was made to allow for interpolyad interactions by extending the rotational matrices to include this Fermi reso-

TABLE III. Rotational constants from least squares fitting of the B^3 polyad of the $\tilde{A}\,^1A_u$ state of C_2H_2. Values are in cm^{-1}. The band origins (T_0) are given relative to T_{00} ($\tilde{A}\,^1A_u$)=42 197.57 cm^{-1}, from Ref. 13. The $J=K=0$ levels lie at 44 457.26 (4^3), 44 547.04 ($4^2 6^1$), 44 547.77 ($4^1 6^2$), and 44 449.15 cm^{-1} (6^3). Derived Coriolis constants: $\zeta^a=0.703_0$, $\zeta_b=0.708_3$; $(\zeta^a)^2+(\zeta^b)^2=0.996$. The parameter A_Δ raises the A constant of $4^2 6^1$ (and lowers that of $4^1 6^2$) relative to its value as interpolated between those for 4^3 and 6^3. The only correlation coefficients with magnitudes over 0.9 are $\frac{1}{2}(B+C)$ (6^3)/$\frac{1}{2}(B+C)$ (4^3) −0.948, A (6^3)/A (4^3) −0.978, and $2A\zeta^a/A_\Delta$ −0.934.

T_0 (4^3)	2295.098	±	0.102	A (6^3)	13.000	±	0.050
T_0 ($4^2 6^1$)	2321.592		0.068	$\frac{1}{2}(B+C)$ (6^3)	1.0870		0.0028
T_0 ($4^1 6^2$)	2314.791		0.087	$(B-C)$ (6^3)	0.1406		0.0072
T_0 (6^3)	2279.470		0.086	A (4^3)	13.121		0.051
$K_{4466}^{(0)}$	−51.019		0.009	$\frac{1}{2}(B+C)$ (4^3)	1.0685		0.0030
$2A\zeta^a$	18.363		0.009	$(B-C)$ (4^3)	0.0798		0.0102
$B\zeta^b$	0.8024		0.0029	$K_{4466,D}$	0.224		0.008
$2A\zeta^a{}_D$	−0.0228		0.00170	A_Δ	−0.398		0.050
			rms error=0.0282 cm^{-1}				

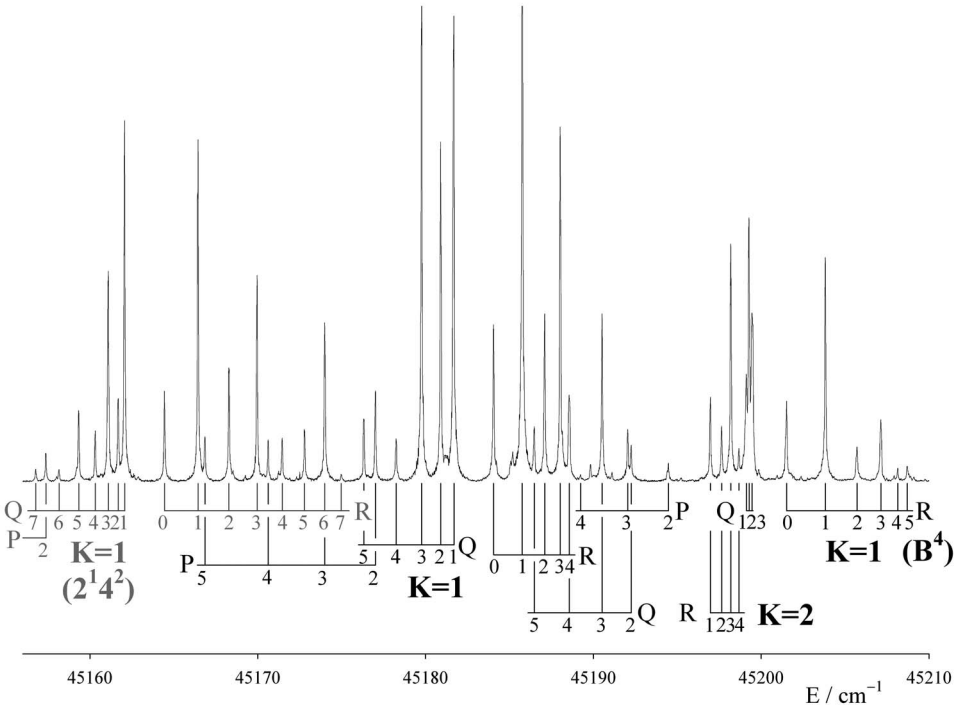

FIG. 8. Three of the lowest energy sub-bands of the B^4 polyad, as seen in one-photon laser excitation. There is a weak Fermi resonance with the $K=1$ level of 2^14^2 (shown in gray).

nance, but the results were inconclusive, presumably because the small perturbation shifts could be absorbed into effective constants for the B^3 polyad. Another factor is that the interpolation of the rotational constants for the combination levels reduces the flexibility of the model. An additional parameter representing a shift in the A rotational constant for the two combination levels, up and down from their interpolated values, was eventually added; it made a considerable improvement to the quality of the fit.

A comparison of Tables II and III shows that the coupling parameters and rotational constants are essentially the same in the B^2 and B^3 polyads, to within their error limits. As was found in the B^2 polyad, the asymmetry parameter $B-C$ is smaller for the 4^3 overtone than for the 6^3 overtone, again suggesting that excitation of the torsional vibration ν_4 makes the molecule significantly nonplanar. The line assignments for the B^3 polyad are included in Table I.

C. The B^4 and B^5 polyads

Given the vibrational and rotational constants from the B^2 and B^3 polyads, the structures of the higher bending polyads can be predicted with fair accuracy. The bands are weak, since higher order anharmonicity terms are required to provide their intensity, but it has been possible to identify portions of both the B^4 and B^5 polyads.

The B^4 polyad consists of five gerade vibrational levels, 4^4, 4^36^1, 4^26^2, 4^16^3, and 6^4, whose $K=0$ rotational levels are calculated to be spread over the energy range of 45 170 $-45\,365$ cm^{-1}. A search of the one-photon LIF spectra immediately identified the two lowest $K'=1$ subbands, within 2 cm^{-1} of their predicted positions, together with a Coriolis-induced $K'=2$ subband. These are illustrated in Fig. 8. Also appearing in Fig. 8 is the top $K'=1$ member of the 2^1B^2 polyad, which is expected to be in Fermi resonance with the B^4 polyad. The fact that the B^4 levels are so close to their expected positions indicates that the effects of the Fermi resonance are quite small. Examination of spectra taken with a warmed beam then allowed identification of the lowest $K'=0$ level and the second $K'=2$ level, as hot bands from ν_4''. These levels lie within 1 cm^{-1} of their predicted positions.

All five $K'=1$ levels of the B^4 polyad can be identified. The two lowest are illustrated in Fig. 8, while the top three lie at 45 276, 45 301, and 45 446 cm^{-1}, all within 1–2 cm^{-1} of their calculated positions. The levels at 45 276 and 45 446 cm^{-1} have not been observed before, but the 45 301 cm^{-1} level, which is almost coincident with the 3^3, $K'=1$ level, had been seen earlier by Scherer *et al.*[55] The 45 301 cm^{-1} level has since been identified as a bending level,[33] but it is now possible to assign it unambiguously as the second-highest $K'=1$ member of the B^4 polyad. The evidence for the assignment is very clear. First, it has essentially no asymmetry splitting. Drabbels *et al.*[56] give the effective value of $B-C$ as $-0.001(3)$ cm^{-1}, while our calculation gives $B-C=0.0006$ cm^{-1}. In comparison, the zero-point level of the $\tilde{A}$ state has $B-C=0.0931$ cm^{-1}. Second, it lies a mere 0.3 cm^{-1} from its predicted position. It can be argued that its position is affected by the presence of the nearby 3^3 level but, since the two levels lie only 0.4 cm^{-1} apart, any shift caused by interaction between them must be small. In fact, a reanalysis[56] of the two interacting levels led to the conclusion that the best fit resulted when the interaction strength was set equal to zero.

No attempt has been made to fit the levels of the B^4

TABLE IV. Calculated $J=K$ rotational levels of the B^4 and B^5 polyads (cm^{-1}). A quantity 1.074 $J(J+1)$ has been subtracted in order to facilitate comparison with Q branch positions in the spectra.

	$K=0$	$K=1e$	$K=1f$	$K=2$
B^4	45 171.80 (a_g)	45 180.76	45 180.79	45 191.23
	45 206.94 (b_g)	45 197.94	45 197.84	45 220.97
	45 239.79 (a_g)	45 275.13	45 275.18	45 266.46
	45 361.62 (b_g)	45 301.63	45 301.63	45 346.16
	45 363.22 (a_g)	45 447.64	45 447.64	45 556.89
B^5	45 894.42 (b_u)	45 896.13	45 896.46	45 912.06
	45 914.48 (a_u)	45 928.16	45 928.18	45 937.90
	46 006.85 (b_u)	45 979.55	45 979.56	46 006.98
	46 017.50 (a_u)	46 076.83	46 076.84	46 058.26
	46 192.59 (b_u)	46 113.30	46 113.30	46 166.75
	46 192.68 (a_u)	46 296.23	46 296.23	46 423.83

polyad by least squares because only eight of the fifteen stacks with $K'=0-2$ have been found, and it is clear that at least two of the stacks are perturbed. For reference, the calculated level pattern is given in Table IV. It is interesting to note how the $K=1$ asymmetry splittings vary erratically in these bending polyads: The pattern in the zero-point level is that the $J=1e$ level lies 0.09 cm^{-1} above the $J=1f$ level, but in the B^4 polyad the $J=1e$ levels are calculated to lie below the $J=1f$ for the lowest two a_g levels, while for the two uppermost $K=1$ levels the asymmetry splitting is close to zero.

The B^5 polyad consists of six ungerade vibrational levels, whose $K'=0$ subbands are calculated to lie in the region of 45 890–46 200 cm^{-1}. This is an extremely crowded region of the double resonance spectrum, where five polyads overlap. Besides B^5, bands are expected from 3^3B^1, 3^15^1, 1^1B^1, and 2^1B^3. The 3^3B^1 polyad gives the most intense bands, and has already been assigned by Mizoguchi *et al.*;[35] the 3^15^1 band has been assigned by Tobiason *et al.*[34] Reasonable predictions can then be made for the K-structures of the other two polyads, based on the properties of the B^1 and B^3 polyads. These indicate that there will be no structure with $K'=0-2$ from overlapping polyads above 46 150 cm^{-1}.

As seen in double resonance via the ground state $\nu_3+\nu_4$ level, the region of 46 150–46 240 cm^{-1} contains six subbands. It is immediately possible to identify three of these as belonging to the B^5 polyad since they lie within 2 cm^{-1} of the positions calculated for them from the constants of the B^2 and B^3 polyads (see Table IV). These three are the close pair of $K'=0$ levels and the $K'=2$ level illustrated in Fig. 9. The calculations predict that the two topmost $K'=0$ levels of the B^5 polyad will form an a_u/b_u pair with the a_u member higher in energy by 0.09 cm^{-1}; what is observed is an a_u/b_u pair with the a_u member higher by 0.3 cm^{-1}. (The small difference between the observed and calculated separations is not considered significant.) The reason why the topmost $K'=0$ levels of a bending polyad form a close pair is that they correlate with what would be the component of highest vibrational angular momentum if the molecule were linear. For such a state a perturbation would only lift the degeneracy in high order.

Given that the predictions of the levels of the B^5 polyad appear to be correct to within a few cm^{-1}, it should be possible to identify more of them in the crowded region at lower energy. Some likely candidates can be picked out, but until the various resonances between the overlapping polyads are better understood a discussion of them would be premature.

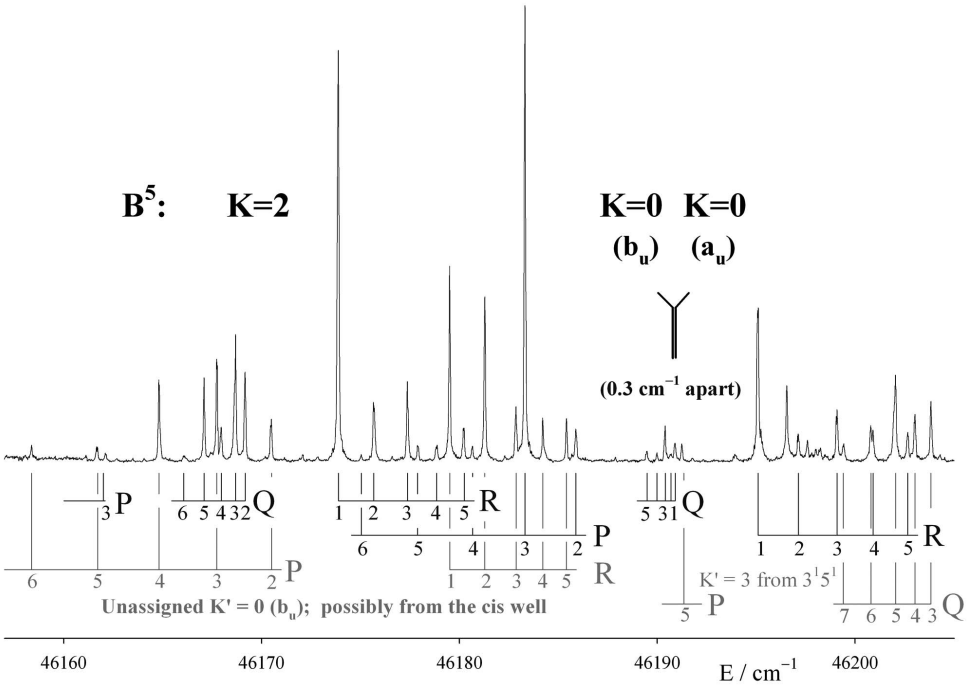

FIG. 9. The two topmost $K=0$ subbands of the B^5 polyad, as seen in IR-UV double resonance via the Q branch of $\nu_3+\nu_4$ at 3897.16 cm^{-1}. These form a very close pair, with the $K'=0$ (a_u) state lying 0.30 cm^{-1} above the $K'=0$ (b_u) state. The R and P branches belong to the b_u state, and the Q branch to the a_u state. Also shown, with assignments marked in black, is the second highest $K'=2$ subband. Two other subbands, marked in gray, are the $K'=3$ subband of 3^15^1 and an unidentified $K'=0$ subband which might possibly represent a level of the S_1 (*cis*-) well.

Two other subbands appear in Fig. 9. One of these is the axis-switching-induced $K'=3$ subband of the $3^1 5^1$ level, the position of which is consistent with the constants for that level given by Tobiason *et al.*[34] The other is a $K'=0$ (b_u) subband at 46 175 cm^{-1}, which seems to be associated with a $K'=2$ subband at 46 227 cm^{-1} (not shown). Near this energy every level of the $\tilde{A}\ ^1A_u$ state that should exist has been accounted for, and it seems that these subbands may represent levels of the *cis*-well of the $\tilde{A}(S_1)$ state, tunneling through the *cis-trans*-isomerization barrier and obtaining some intensity through interaction with nearby levels of the *trans*-well. These levels will be discussed further in a subsequent paper.

V. DISCUSSION

In this work detailed rotational analyses of the pure bending polyads with $v_4+v_6=2$ and 3 have been carried out for the $\tilde{A}\ ^1A_u$ state of acetylene. The $v_4+v_6=2$ polyad (B^2) was recorded as high sensitivity one-photon laser-induced fluorescence spectra, while the $v_4+v_6=3$ polyad (B^3) was recorded by IR-UV double resonance, using the ground state ν_3 fundamental and the $\nu_3+\nu_4$ combination level as intermediates. The bands are weak because they are Franck–Condon forbidden; their intensity comes from anharmonic mixing of their upper states with the Franck–Condon allowed levels of the 3^n and $2^1 3^n$ progressions.

The structures of the higher bending polyads are unexpectedly complicated because, in addition to the Coriolis coupling that was recognized[33] in the fundamentals, they suffer from unusually strong Darling–Dennison resonance, where the parameter K_{4466} is no less than -51 cm^{-1}. Its effect is that, even for $K=0$, the members of a polyad with the same vibrational symmetry are pushed apart by amounts of the order of 50–100 cm^{-1}, even though the fundamentals themselves are almost degenerate. For $K \geqslant 1$ the *a*-axis Coriolis coupling causes the vibrational levels with different symmetries to interact with each other, following $\Delta K=0$ selection rules, while the *b*-axis Coriolis coupling causes local interactions between close-lying levels with different *K*-values.

An interesting result of the strong *a*-axis Coriolis coupling is that the asymmetry splitting in the higher $K=1$ members of a bending polyad is almost zero. The reason for this is that their wave functions contain nearly equal mixtures of basis states with *a* and *b* vibrational symmetries. The *e*/*f* energy order of the $K=1$ asymmetry components is opposite in vibrational levels with *a* and *b* symmetries, so that the equal and opposite asymmetry splittings cancel in the heavily Coriolis-mixed levels.

As can be seen from Eqs. (9) and (11), the strengths of the Coriolis coupling and the Darling–Dennison resonance both depend on the vibrational quantum numbers, which means that they become extremely large in the higher polyads. Nevertheless the dependence is perfectly regular, so that it is possible to predict the level structures of the polyads with $v_4+v_6=4$ and 5 with good accuracy, and to identify some of their *K*-stacks. The bands involved are extremely weak, as might be expected since the intensity is transferred to them from the Franck–Condon allowed bands only by high order mixing terms. Once allowance is made for the Darling–Dennison resonance, the pure bending vibrational motion is found to be comparatively harmonic. The underlying level structure can be represented by the following constants:

$$\omega_4 = 764.71, \quad \omega_6 = 772.50, \quad x_{44} = 0.19,$$
$$x_{66} = -4.23, \quad x_{46} = 11.39\ cm^{-1}, \tag{16}$$

where, as discussed below, the value of x_{46} arises mostly from the Coriolis coupling.

The Coriolis coupling is a symptom that vibrational angular momentum is present. As Eq. (16) shows, the two bending vibrations ν_4 and ν_6 have almost the same frequency. If the molecule were linear they would coalesce into the degenerate *cis*-bending vibration (ν_5, π_u) of the linear configuration, with its associated vibrational angular momentum. This angular momentum does not go away in the bent molecule, but instead appears as a coupling of the two nearly degenerate vibrations: In the rotational structure it gives rise to the *a*- and *b*-axis Coriolis coupling, while in the vibrational structure it adds to the Darling–Dennison resonance parameter K_{4466} and the anharmonicity parameter x_{46}. Remarkably, the vibrational angular momentum contributes the larger portion of both these parameters, which are usually considered to be mostly anharmonic. Specifically, it adds a quantity $2[A(\zeta_{46}^{a})^2+B(\zeta_{46}^{b})^2]=14.1$ cm^{-1} to x_{46}, and -2 times this quantity to K_{4466}. The zeta sum rule, given as Eq. (5), is found to hold very accurately in the bending polyads.

The analysis of the lowest bending polyads of the $\tilde{A}\ ^1A_u$ state has important consequences for the understanding of the higher vibrational levels, particularly for those approaching the barrier to *cis-trans*-isomerization. A significant result is that the singlet state vibrational level which appears to interact[49] with the low-*J* levels of the 3^3, $K'=1$ stack can now be definitely assigned. This state had been found to interact via $\Delta K=0$ selection rules,[49] albeit with a very small interaction matrix element,[50] suggesting that the mechanism involves *a*-axis Coriolis coupling or Fermi resonance. Based on their measurement of the ν_4 and ν_6 fundamentals, Utz *et al.* suggested[33] that the interacting state was one of the vibrationally a_g members of the B^4 polyad, 4^4, $4^2 6^2$, or 6^4. With the accurate simulation of the B^4 polyad available from the present work, the interacting level is now seen to be the second-highest $K=1$ member of the B^4 polyad. This is a combination level with nominal b_g vibrational symmetry, though the strength of the *a*-axis Coriolis coupling is so great in this polyad that for $K>0$ the resulting levels are complete mixtures of a_g and b_g vibrational basis states.

The patterns found in the B^2 and B^3 pure bending polyads can be extended to the analyses of combination polyads such as $2^1 B^2$ and $3^1 B^2$. Among the interesting results is that the 1^1 fundamental is found to lie in the middle of the $2^1 B^2$ polyad, and to interact strongly with it; the resulting rotational structure is very disorganized, but analysis has led to a direct determination of the ν_1 fundamental frequency. These results are described in a following paper.[57]

ACKNOWLEDGMENTS

We thank Annelise R. Beck for her assistance in collecting the LIF data at M.I.T. For partial support of this work one of the authors (A.J.M.) thanks the Natural Sciences and Engineering Research Council of Canada, another author (N.Y.) thanks the Asian CORE Program for Molecular Science, and another (S.T.) thanks the National Science Council of Taiwan. At M.I.T. the work was supported by DOE Grant No. DE-FG0287ER13671.

[1] G. W. King and C. K. Ingold, Nature (London) **169**, 1101 (1952).
[2] C. K. Ingold and G. W. King, J. Chem. Soc. **1953**, 2702.
[3] K. K. Innes, J. Chem. Phys. **22**, 863 (1954).
[4] D. Demoulin and M. Jungen, Theor. Chim. Acta **34**, 1 (1974).
[5] H. Lischka and A. Karpfen, Chem. Phys. **102**, 77 (1986).
[6] Y. Yamaguchi, G. Vacek, and H. F. Schaefer, Theor. Chim. Acta **86**, 97 (1993).
[7] G. Vacek, J. R. Thomas, B. J. DeLeeuw, and Y. Yamaguchi, J. Chem. Phys. **98**, 4766 (1993).
[8] J. F. Stanton, C. Huang, and P. G. Szalay, J. Chem. Phys. **101**, 1 (1994).
[9] C. D. Sherrill, G. Vacek, Y. Yamaguchi, H. F. Schaefer III, J. F. Stanton, and J. Gauss, J. Chem. Phys. **104**, 8507 (1996).
[10] K. Malsch, R. Regentisch, P. Swiderek, and G. Hohlneicher, Theor. Chem. Acc. **100**, 171 (1998).
[11] E. Ventura, M. Dallos, and H. Lischka, J. Chem. Phys. **118**, 1702 (2003).
[12] D. H. Mordaunt and M. N. R. Ashfold, J. Chem. Phys. **101**, 2630 (1994).
[13] J. K. G. Watson, M. Herman, J. C. Van Craen, and R. Colin, J. Mol. Spectrosc. **95**, 101 (1982).
[14] J. C. Van Craen, M. Herman, R. Colin, and J. K. G. Watson, J. Mol. Spectrosc. **111**, 185 (1985).
[15] T. R. Huet, M. Godefroid, and M. Herman, J. Mol. Spectrosc. **144**, 32 (1990).
[16] J. T. Hougen and J. K. G. Watson, Can. J. Phys. **43**, 298 (1965).
[17] J. C. Van Craen, M. Herman, R. Colin, and J. K. G. Watson, J. Mol. Spectrosc. **119**, 137 (1986).
[18] S. A. B. Solina, J. P. O'Brien, R. W. Field, and W. F. Polik, J. Phys. Chem. **100**, 7797 (1996).
[19] M. P. Jacobson, J. P. O'Brien, R. J. Silbey, and R. W. Field, J. Chem. Phys. **109**, 121 (1998).
[20] M. P. Jacobson and R. W. Field, J. Phys. Chem. **104**, 3073 (2000).
[21] K. Hoshina, A. Iwasaki, K. Yamanouchi, M. P. Jacobson, and R. W. Field, J. Chem. Phys. **114**, 7424 (2001).
[22] K. Tsuji, C. Terauchi, K. Shibuya, and S. Tsuchiya, Chem. Phys. Lett. **306**, 41 (1999).
[23] B. J. Orr, Int. Rev. Phys. Chem. **25**, 655 (2006).
[24] D. M. Jonas, S. A. B. Solina, B. Rajaram, R. J. Silbey, R. W. Field, K. Yamanouchi, and S. Tsuchiya, J. Chem. Phys. **99**, 7350 (1993).
[25] D. J. Nesbitt and R. W. Field, J. Phys. Chem. **100**, 12735 (1996).
[26] D. B. Moss, Z. Duan, M. P. Jacobson, J. P. O'Brien, and R. W. Field, J. Mol. Spectrosc. **199**, 265 (2000).
[27] M. Silva, R. Jongma, R. W. Field, and A. M. Wodtke, Annu. Rev. Phys. Chem. **52**, 811 (2001).
[28] J. K. Lundberg, Y. Chen, J. P. Pique, and R. W. Field, J. Mol. Spectrosc. **156**, 104 (1992).
[29] M. Takahashi, M. Fujii, and M. Ito, J. Chem. Phys. **96**, 6486 (1992).
[30] J. K. Lundberg, D. M. Jonas, B. Rajaram, Y. Chen, and R. W. Field, J. Chem. Phys. **97**, 7180 (1992).
[31] S. T. Pratt, P. M. Dehmer, and J. L. Dehmer, J. Chem. Phys. **99**, 6233 (1993).
[32] S.-J. Tang, Y.-C. Chou, J. J.-M. Lin, and Y.-C. Hsu, J. Chem. Phys. **125**, 133201 (2006).
[33] A. L. Utz, J. D. Tobiason, E. Carrasquillo, L. J. Sanders, and F. F. Crim, J. Chem. Phys. **98**, 2742 (1993).
[34] J. D. Tobiason, A. L. Utz, and F. F. Crim, J. Chem. Phys. **99**, 928 (1993).
[35] M. Mizoguchi, N. Yamakita, S. Tsuchiya, A. Iwasaki, K. Hoshina, and K. Yamanouchi, J. Phys. Chem. A **104**, 10212 (2000).
[36] A. J. Merer, N. Yamakita, S. Tsuchiya, J. F. Stanton, Z. Duan, and R. W. Field, Mol. Phys. **101**, 663 (2003).
[37] F. Hegelund, H. Bürger, and O. Polanz, J. Mol. Spectrosc. **167**, 1 (1994).
[38] B. T. Darling and D. M. Dennison, Phys. Rev. **57**, 128 (1940).
[39] E. B. Wilson and J. B. Howard, J. Chem. Phys. **4**, 260 (1936).
[40] E. B. Wilson, J. C. Decius, and P. C. Cross, *Molecular Vibrations* (McGraw-Hill, New York, 1955).
[41] J. K. G. Watson, Mol. Phys. **15**, 479 (1968).
[42] T. Oka and Y. Morino, J. Mol. Spectrosc. **6**, 472 (1961).
[43] C. di Lauro and I. M. Mills, J. Mol. Spectrosc. **21**, 386 (1966).
[44] I. M. Mills, Pure Appl. Chem. **11**, 325 (1965).
[45] K. K. Lehmann, J. Chem. Phys. **79**, 1098 (1983).
[46] M. S. Child and L. Halonen, Adv. Chem. Phys. **57**, 1 (1984).
[47] I. M. Mills and A. G. Robiette, Mol. Phys. **56**, 743 (1985).
[48] K. K. Lehmann, J. Chem. Phys. **96**, 8117 (1992).
[49] K. K. Lehmann, Mol. Phys. **66**, 1129 (1989).
[50] W. Gordy and R. L. Cook, *Microwave Molecular Spectra* (Wiley, New York, 1984).
[51] R. N. Dixon and N. G. Wright, Chem. Phys. Lett. **117**, 280 (1985).
[52] A. Held, B. B. Champagne, and D. W. Pratt, J. Chem. Phys. **95**, 8732 (1991).
[53] I. M. Mills, *Molecular Spectroscopy: Modern Research*, edited by K. N. Rao and C. W. Mathews (Academic, New York, 1972), Chap. 3.2.
[54] G. Winnewisser, M. Winnewisser, and W. Gordy, J. Chem. Phys. **49**, 3465 (1968).
[55] G. J. Scherer, Y. Chen, R. L. Redington, J. L. Kinsey, and R. W. Field, J. Chem. Phys. **85**, 6315 (1986).
[56] M. Drabbels, J. Heinze, and W. L. Meerts, J. Chem. Phys. **100**, 165 (1994).
[57] A. H. Steeves, A. J. Merer, H. A. Bechtel, A. R. Beck, and R. W. Field, "Direct observation of the symmetric stretching modes of $\tilde{A}\,^1A_u$ acetylene by pulsed supersonic jet laser induced fluorescence" (unpublished).